Neutronics/Thermo-fluid Coupled Analysis of PMR-200 Equilibrium Cycle by CAPP/GAMMA+ Code System

Hyun Chul Lee *, Nam-il Tak
Korea Atomic Energy Research Institute, 111 Daedeok-daero 989 Beon-gil, Yuseong-gu, Daejeon 305-353, Korea
**Corresponding author: lhc@kaeri.re.kr*

1. Introduction

A coupled code system for neutronics/thermos-fluid coupled analysis of VHTR core, CAPP/GAMMA+ [1], was developed at KAERI. The CAPP code is a 3-dimensional nodal code for VHTR core physics analysis and simulation [2] and the GAMMA+ code is a system/safety analysis code for thermo-fluid and system transient of VHTR [3].

In this paper, steady-state performance of the equilibrium core of PMR-200 was analyzed using the CAPP/GAMMA+ coupled code system. The equilibrium core was obtained by performing CAPP stand-alone multi-cycle depletion calculation with critical rod position search.

2. Coupled Code System

2.1 CAPP Code

The CAPP code solves the multi-group neutron diffusion equation based on the finite element method. Fig. 1 shows the block nodalization and the finite elements. A block is divided into six triangular prisms radially and each of them is axially divided into several homogeneous zones. A triangular prismatic finite element is assigned for each homogeneous zone. The microscopic cross-sections are represented as a function of burnup, moderator temperature, and fuel temperature in the CAPP code. Micro depletion calculation with the user-defined nuclide chain is performed for each homogeneous zone by using the one-group cross-sections and the one-group flux determined by the neutron flux solver.

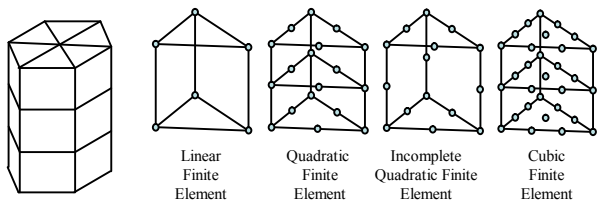

Fig. 1. Block nodalization and finite elements.

2.2 GAMMA+ Code

The GAMMA+ code has the capability of multi-dimensional multi-component mixture analysis to investigate various phenomena of a high temperature gas cooled reactor such as pressurized or depressurized conduction cool down and air/water-ingress accidents.

For fluid, the continuity (or mass conservation) equation, momentum conservation equation, energy conservation equation, and species conservation equation are solved simultaneous. Three different scales of heat conduction models are used in GAMMA+. These are (1) a heat conduction model in TRISO particles, (2) an implicit heat conduction model between TRISO particles and the fuel compact, and (3) a multi-dimensional heat conduction model with fuel or reflector blocks.

2.3 Code Coupling

Fig. 2 shows the CAPP/GAMMA+ coupling scheme. A server program named INTCA is used to control the coupled calculation of CAPP and GAMMA+. The CAPP code calculates the power density and the fast fluence and sends them to GAMMA+. The power density data are used as heat source in GAMMA+. The fast fluence is used for evaluating the conductivity of graphite material. On the other hand, GAMMA+ calculates core temperatures and sends them to CAPP. The temperature data are used to evaluate nuclear cross-sections in CAPP. The nuclide number densities in Fig. 2 will be used in the accident conditions such as air/water-ingress.

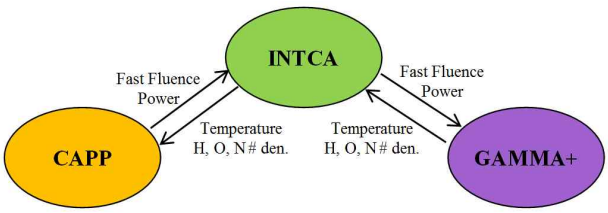

Fig. 2. CAPP/GAMMA+ Coupling Scheme.

The computational cells of the CAPP and GAMMA+ codes do not necessarily match exactly because the GAMMA+ code uses either hexagonal or triangular radial cells while the CAPP code uses triangular radial cells. So, mappings between the variables in the two codes are required and INTCA provide the mapping between the two codes.

INTCA controls the two codes by receiving the requests from the two codes and sending the commands

to the two codes. The control algorithms of the three codes are explained in detail in reference 1.

3. Numerical Results

Fig. 3 shows the CAPP nodalization for the reactor core of PMR-200 [4]. One third of the core was modeled with a rotational symmetry. Although the side reflector of PMR-200 has a cylindrical outer boundary, the side reflector was modeled as if it were composed of hexagonal reflector blocks. As a consequence, the mapping between the cells of the CAPP code and those of the GAMMA+ code is not exact at the periphery of the side reflector. However, the importance of the periphery of the side reflector is small enough in the neutronics calculation. There are four reserved shutdown holes and four start-up control rod holes in the 1/3 sector of the active core region and the holes are empty during operation. There are eight operating control rods in the 1/3 sector of the side reflector region. They are grouped into four control banks as shown in Fig 3(a). It was assumed that the banks are inserted without overlapping, which means that the n^{th} bank starts to move after the $(n\text{-}1)^{th}$ bank is fully inserted. All the blocks are divided into six triangles radially and two zones axially. Only axial shuffling of the fuel blocks is adopted for refueling as shown in Fig 3(b).

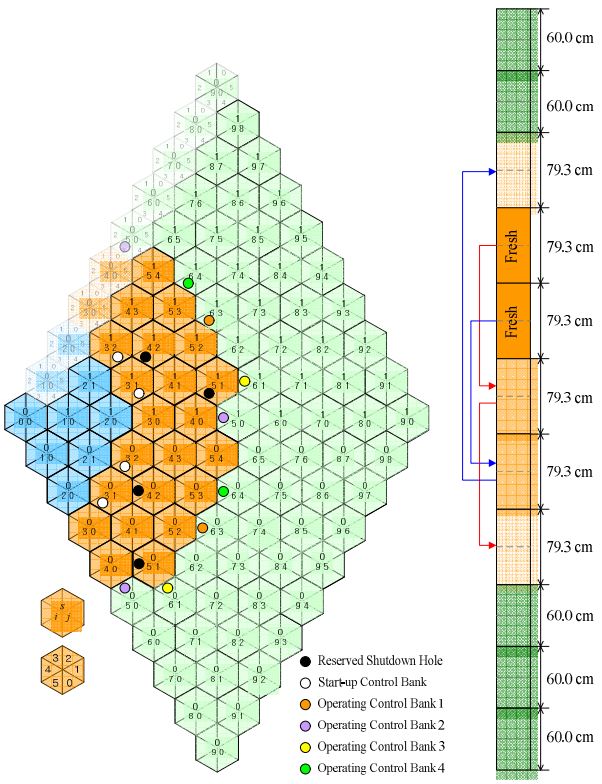

(a) Radial configuration (b) Axial configuration

Fig. 3. Core configuration of PMR-200 for CAPP.

Fig. 4 shows the GAMMA+ nodalization for the PMR-200 core. Due to symmetry, 1/3 section of the core was considered. Single fuel column was modeled by six triangular cells. In the case of reflector columns, either hexagonal or triangular cells were adopted. The coolant and bypass gap channels were grouped to reduce the number of the computational cells while all the control rod channels were individually modeled. For example, single coolant channel was modeled for the triangular region of fuel column. That is, 18 coolant channels in the same triangular region were grouped into one coolant channel. In terms of the axial aspect, one cell was assigned for the each fuel block.

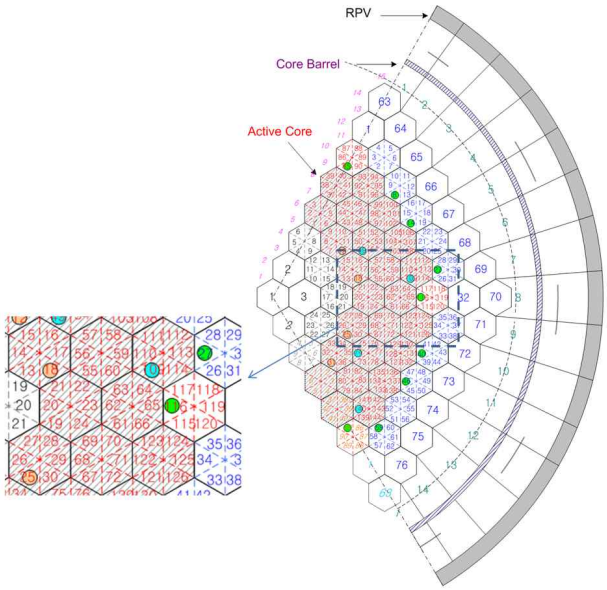

Fig. 4. PMR-200 reactor configuration for GAMMA+.

The steady-state performance of the equilibrium core of PMR-200 was analyzed using the CAPP/GAMMA+ coupled code system. The equilibrium core was obtained by performing CAPP stand-alone multi-cycle depletion calculation with critical rod position search. The axial shuffling scheme shown in Fig. 3(b) was adopted for reloading of the fuel blocks and the cycle length of 450 effective full power days (EFPDs) was achieved. In the CAPP stand-alone calculation for searching for the equilibrium core, the imbedded thermo-fluid solver in the CAPP code was used to calculate the temperature for thermal feedback. Two types of depletion calculation were performed. One is a depletion calculation with reactivity search and the other is a depletion calculation with critical rod position search. The two codes exchanged coupling data at every 15.0 sec in GAMMA+ problem time during the coupled calculation. The coupled calculations continued until the maximum temperature change and the maximum power density change were below 10^{-3} and 10^{-4}, respectively.

3.1 Core Depletion Calculation with Reactivity Search

In this coupled core depletion calculation, the multiplication factor of the core was evaluated at every burnup step of the equilibrium cycle of PMR-200 from the beginning of cycle (BOC) to the end of cycle (EOC). Once the converged multiplication factor of the core was obtained at a burnup step, the depletion calculation was performed for the next burnup step.

Fig. 5 shows the excess reactivity at hot full power state during the equilibrium cycle. The excess reactivity at BOC for no Xe condition (0 EFPD) and equilibrium Xe condition (3 EFPDs) are 4158 pcm and 1975 pcm, respectively and the corresponding Xe worth is -1864 pcm. The excess reactivity increases up to 4148 pcm at 200 EFPDs as the B4C burnable poison burns out and then decreases to near zero at EOC due to the depletion of nuclear fuel and the accumulation of fission products.

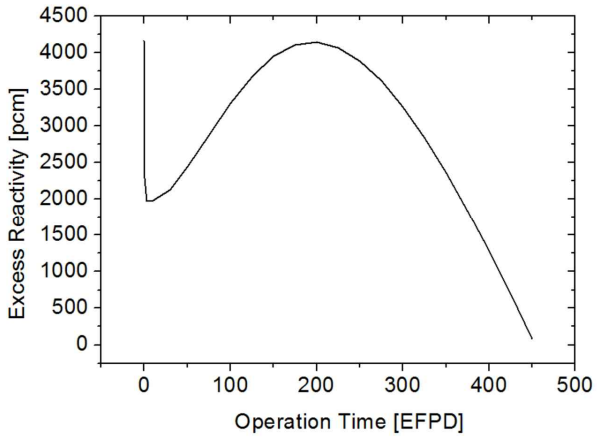

Fig. 5. Excess reactivity during the equilibrium cycle.

3.2 Core Depletion Calculation with Critical Control Rod Position Search

In this coupled depletion calculation, the critical control rod positions were searched at every burnup step of the equilibrium cycle of PMR-200 from BOC to EOC. Once the converged multiplication factor of the core was obtained, the control rod positions were adjusted based on the multiplication factor obtained to make the reactor critical. After a criticality of the reactor was achieved at a burnup step, the depletion calculation was performed for the next burnup step.

Fig. 6 shows the critical control rod positions for the four banks shown in Fig. 3(a). The rod position is defined as the control rod tip position from the bottom of the active core. At BOC no Xe state, bank 1 and 2 are fully inserted and bank 3 is partially inserted. Bank 3 followed by bank 2 is withdrawn to compensate for the Xe worth as the Xe builds up. Bank 2 followed by bank 3 is again inserted to compensate for the burn out of the burnable poison. Bank 3 followed by bank 2 and 1 is withdrawn as the excess reactivity decreases due to depletion of nuclear fuel and the accumulation of fission products. Bank 4 remains fully withdrawn during the whole cycle.

Fig. 7 compares the axially averaged radial power density profiles at BOC equilibrium Xe condition, MOC (middle of cycle), and EOC. At BOC and MOC the radial power is skewed toward the inner ring because the control rods are inserted in the side reflector region but the radial power is slightly skewed toward the outer ring at EOC because of the withdrawal of the control rods in the side reflector region. Fig. 8 shows radially averaged axial power density profile at BOC, MOC, and EOC. At BOC, the axial power is almost symmetric but the axial power is strongly skewed toward the top of the core at MOC and EOC due to the combined effect of the control rod movement and the burn out of the burnable poison in the fresh fuel. Fig. 9 shows the axial offset history during the equilibrium cycle. The axial power remains top-skewed during most of the operation time of the equilibrium cycle except for the BOC.

Fig. 10 compares the radial temperature profiles at BOC, MOC, and EOC. The fuel temperature was plotted in the active core region while the graphite temperature was plotted in the reflector region. For BOC and MOC, the fuel temperature of the inner ring is higher since the power density of the inner ring is higher as shown in Figs. 7(a) and 7(b). In particular, Fig. 10(b) shows the existence of a steep temperature gradient due to a steep gradient of the power density. Fig. 10(c) shows that the temperature profile of EOC is relatively flat due to the flat power density profile. Fig. 11 compares the radially averaged axial fuel temperature profile at BOC, MOC, and EOC. The axial fuel temperature profiles at MOC and EOC are similar to each other while they are quite different from those at BOC, which is attributed to the fact that the axial power profiles at MOC and EOC are similar but they are different from those at BOC.

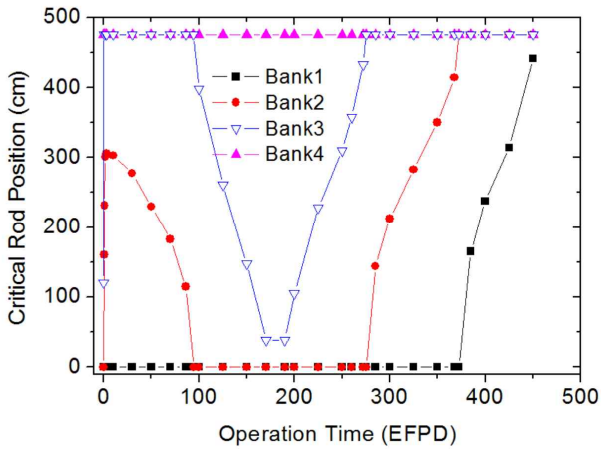

Fig. 6. Critical control rod position during the equilibrium cycle.

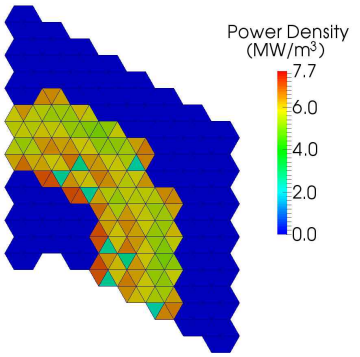

(a) BOC(Eq.Xe)

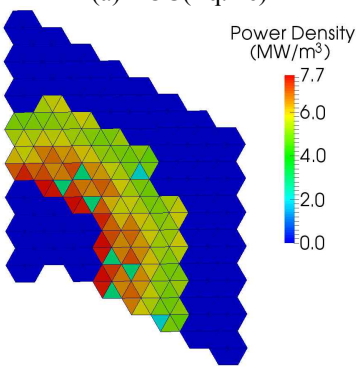

(b) MOC

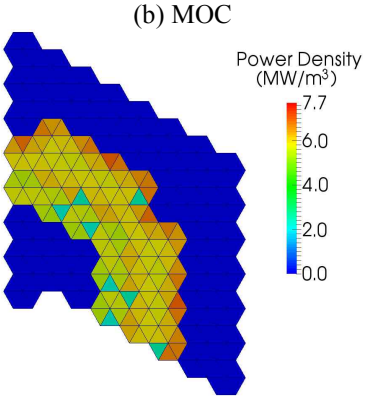

(c) EOC

Fig. 7. Axially averaged radial power density profile.

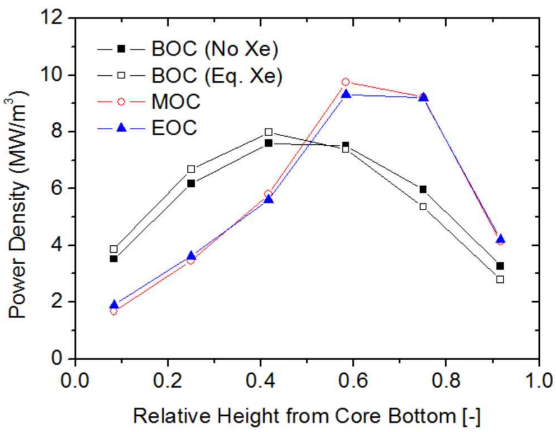

Fig. 8. Radially averaged axial power density profile.

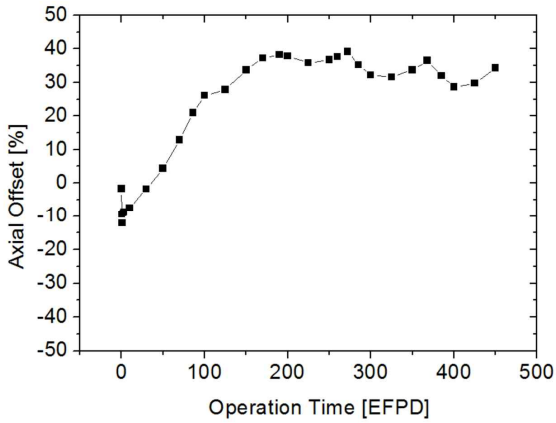

Fig. 9. Axial offset during the equilibrium cycle.

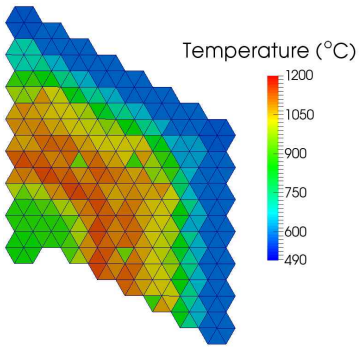

(a) BOC(Eq.Xe)

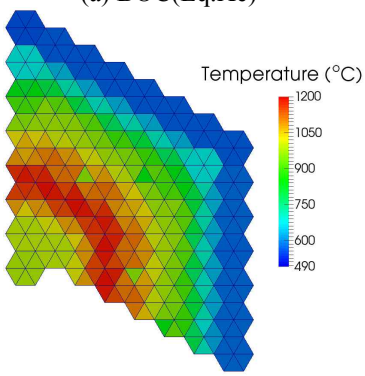

(b) MOC

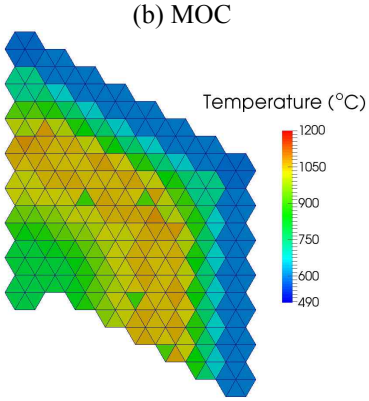

(c) EOC

Fig. 10. Radial temperature distribution at the bottom layer of the active core.

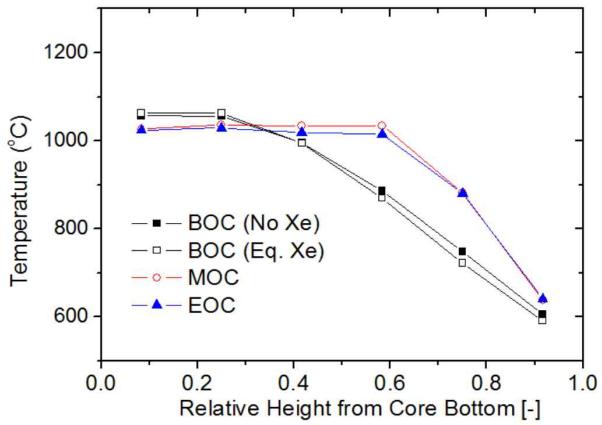

Fig. 11. Radially averaged axial fuel temperature profile.

3.3 Effect of Bypass Flow

In this section, the effect of bypass flow was investigated. In order to examine the effect of bypass flow, the bypass gap in the GAMMA+ model was removed and the coupled simulation was repeated for the BOC of PMR-200 equilibrium cycle. The results of the CAPP/GAMMA+ coupled calculation with and without bypass model are summarized in Table 1. The temperatures of the active core region were slightly decreased since more coolant flows through the coolant channels. On the other hand, the temperatures of the central and side reflectors were increased since there was no convection flow. In particular, the temperature of the central reflector was dramatically increased. The multiplication factor was increased by 316 pcm without the bypass flow as a combined effect of the temperature changes in active core and the reflector region. It is well known that the reflector temperature coefficient is positive while the fuel temperature coefficient and the moderator coefficient are negative. The both effects of the temperature change in the two regions increase the reactivity.

Table I: Effect of bypass flow on the core performance

	With bypass flow	Without bypass flow
Effective multiplication factor	1.04338	1.04654
Avg. fuel temp. (°C)	888	867
Avg. moderator temp. (°C)	878	856
Avg. top reflector temp. (°C)	494	494
Avg. bottom reflector temp. (°C)	987	955
Avg. central reflector temp. (°C)	713	831
Avg. side reflector temp. (°C)	622	665

Fig. 12 shows the effect of bypass flow on the axially averaged radial power density profile. No big difference is seen. Fig. 13 shows the effect of bypass flow on the radially averaged axial power density profile. It is obvious that the effect of the bypass flow on the axial power density profile is small. Fig. 14 shows the effect of bypass flow on the radial temperature profile at BOC. The dramatically increased central reflector temperature can be observed. Fig. 15 shows the effect of bypass flow on the radially averaged axial fuel temperature profile. A slight decrease in the temperature profile can be seen in the case of without bypass flow. The difference is gradually increased toward the outlet of the core. This can be explained that more coolant flow goes through the core in the case without bypass flow.

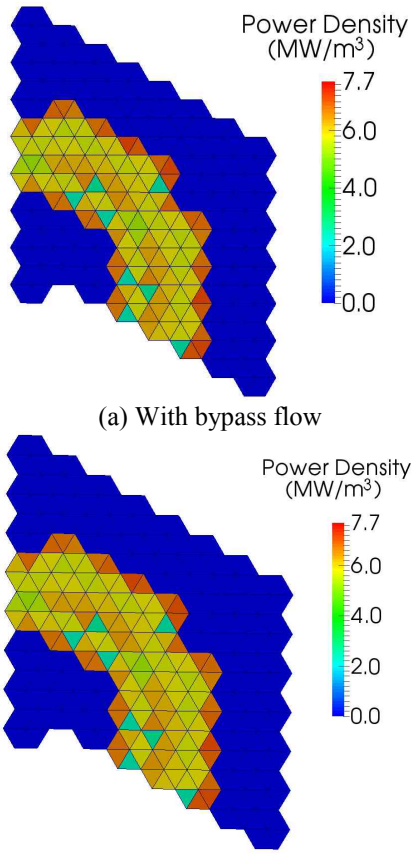

(a) With bypass flow

(b) Without bypass flow

Fig. 12. Effect of bypass flow on the radial power density profile.

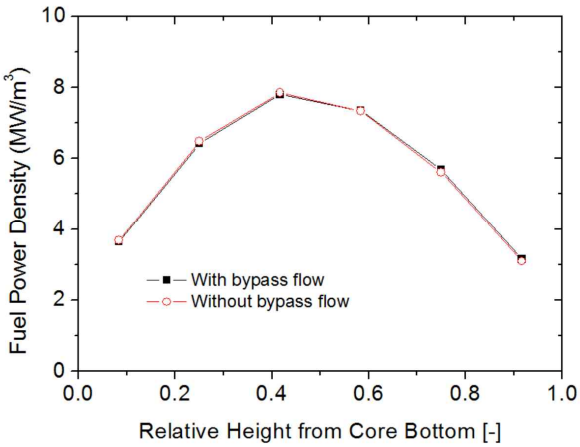

Fig. 13. Effect of bypass flow on the axial power density profile.

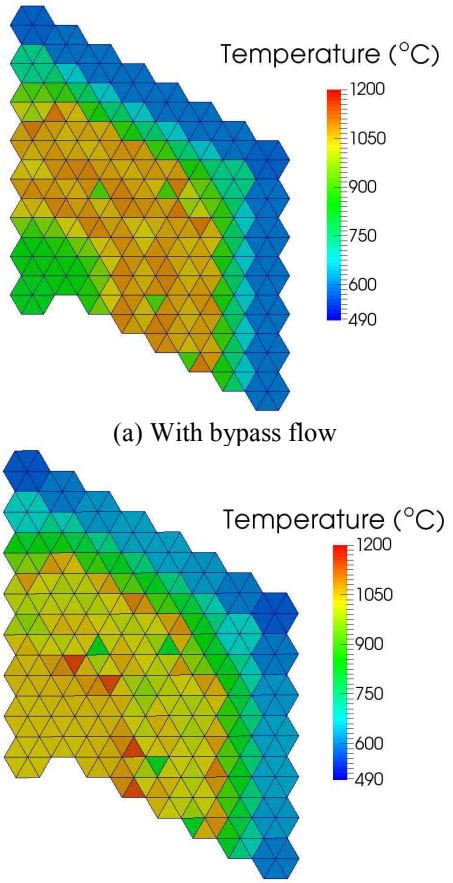

(a) With bypass flow

(b) Without bypass flow

Fig. 14. Effect of bypass flow on the radial temperature profile.

4. Conclusions

In this work, a code system for coupled neutronics and thermo-fluids simulation was developed using CAPP and GAMMA+ codes. A server program, INTCA, controls the two codes for coupled calculations and performs the mapping between the variables of the two codes based on the nodalization of the two codes.

In order to extend the knowledge about the coupled behavior of a prismatic VHTR, the CAPP/GAMMA+ code system was applied to steady state performance analysis of PMR-200. The coupled calculation was carried out for the equilibrium core of PMR-200 from BOC to EOC. The peak fuel temperature was predicted to be 1372 oC near MOC. However, the cycle-average fuel temperature was calculated as 1230 oC, which is slightly below the design target of 1250 oC.

In addition, significant impact of the bypass flow on the central reflector temperature was found. Without bypass flow, the temperature of the active core region was slightly decreased while the temperature of the central and side reflector region was increased much. The both changes in the temperature increase the multiplication factor and the total change of the multiplication factor was more than 300 pcm. On the other hand, the effect of the bypass flow on the power density profile was not significant.

It is envisaged that transient calculations such as loss of forced convection and water-ingress will be performed with the present coupled code system.

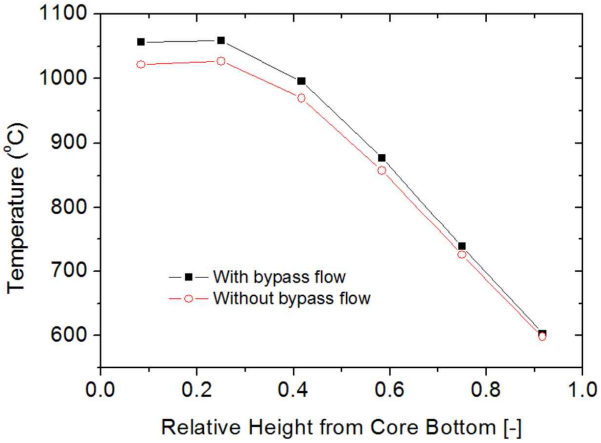

Fig. 15. Effect of bypass flow on the axial fuel temperature profile.

Acknowledgements

This work was supported by Nuclear R&D Program of the NRF of Korea grant funded by the Korean government (Grant code: NRF-2012M2A8A2025679).

REFERENCES

[1] H. C. Lee and N. Tak, "Development of CAPP/GAMMA+ Code System for Neutronics/Thermo-fluid Coupled Analysis of a Prismatic VHTR Core," Proceedings of the Reactor Physics Asia 2015 Conference, Sept. 17-18, 2015, Jeju, Korea.
[2] H. C. Lee et al., "CAPP v2.1 user's manual," KAERI/TR-5334/2013 (2013).
[3] H. S. Lim et al., "GAMMA multidimensional multi-component mixture analysis to predict air ingress phenomena in an HTGR," Nucl. Sci. Eng. 152, 87-97 (2006).
[4] H. C. Lee et al., "Decay heat analysis of VHTR cores by Monte Carlo core depletion calculation," Annals of Nuclear Energy, 37, 1356-1368. (2010).